Journal of
Materials Chemistry C

PAPER

View Article Online
View Journal | View Issue

Open Access Article. Published on 08 July 2016. Downloaded on 1/16/2026 9:49:37 PM.
This article is licensed under a Creative Commons Attribution 3.0 Unported Licence.

Cite this: J. Mater. Chem. C, 2016, 4, 7026

# Ultraviolet and blue cathodoluminescence from cubic $Y_2O_3$ and $Y_2O_3$:$Eu^{3+}$ generated in a transmission electron microscope

D. den Engelsen,[a] G. R. Fern,[a] T. G. Ireland,*[a] P. G. Harris,[a] P. R. Hobson,[b] A. Lipman,[a] R. Dhillon,[a] P. J. Marsh[a] and J. Silver[a]

Received 29th April 2016,
Accepted 5th July 2016

DOI: 10.1039/c6tc01750a

www.rsc.org/MaterialsC

Herein we describe the investigation of cubic spherical submicron particles of non-doped $Y_2O_3$ and $Y_2O_3$ doped with $Eu^{3+}$ in a transmission electron microscope (TEM) equipped with a spectrometer to detect cathodoluminescence from individual particles. Each submicron particle was made up of nanometre sized crystals. We found that these crystals showed a broad emission band at 353 nm upon bombardment with 200 keV or 80 keV electrons. Upon increasing the $Eu^{3+}$ concentration from 0 to 2 mol% this UV/blue emission was gradually quenched: at $Eu^{3+}$ concentrations >2 mol% no UV/blue emission was detected, only the well-known cathodoluminescence (CL) spectrum of $Y_2O_3$:$Eu^{3+}$ could be recorded. This UV/blue emission has been attributed to the intrinsic luminescence of $Y_2O_3$ caused by self-trapped excitons. We found that the UV/blue luminescence was strongly temperature dependent and that the trap depth of the self-trapped excitons was 0.14 eV. The ratios of the spectral radiances of $^5D_1 \rightarrow {}^7F_J$ and $^5D_0 \rightarrow {}^7F_J$ ($J$ = 0, 1...6) $Eu^{3+}$ transitions in the CL-TEM spectra of $Y_2O_3$:$Eu^{3+}$ at low $Eu^{3+}$ concentrations was about a factor of 10 larger than those recorded at 15 keV. This phenomenon has been explained by absorption of the intrinsic luminescence of $Y_2O_3$ by $Eu^{3+}$.

## 1. Introduction

Yttrium oxide ($Y_2O_3$:$Eu^{3+}$) is a well-known phosphor from its application as the red emitting phosphor in fluorescent lamps and projection cathode ray tubes (CRTs).[1–3] Due to the industrial applications and the attractive properties of $Y_2O_3$ as host lattice, $Y_2O_3$ doped with $Eu^{3+}$ and other rare earth ions has been well studied and documented. The expected application of $Y_2O_3$:$Eu^{3+}$ in low-voltage field emission displays has stimulated intensive research in the synthesis and characterisation of nanosized phosphors, recently reviewed by Li and Lin.[4] In our laboratory we have studied the enhancement of cathodoluminescence by applying double layers of ZnO:Zn and $Y_2O_3$:$Eu^{3+}$.[5] Non-doped $Y_2O_3$ also yields photoluminescence when excited with UV radiation. Although this has been known for more than 50 years,[6] the luminescence of non-doped $Y_2O_3$ has not been studied in much detail until recently. The reason for this recent interest is the possible application of non-doped $Y_2O_3$ and $Y_2O_3$ doped with $Eu^{3+}$, $Tb^{3+}$, $Nd^{3+}$ or $Tm^{3+}$ as a scintillation material.[7–15] When non-doped $Y_2O_3$ is excited by α-particles,[7] UV-radiation (207 nm)[8] or X-rays,[9–13] a broad luminescence band is observed between 340 nm and 500 nm. Table 1 summarizes the wavelength at maximum ($\lambda_{max}$) of this broad luminescence band recorded in the literature. The values for $\lambda_{max}$ listed in Table 1 vary substantially. This erratic behaviour of the luminescence of $Y_2O_3$ elicited the following statement from Fukabori *et al.*[7] "Light yields of $Y_2O_3$ ceramics are different from specimen to specimen. Nature of this phenomenon is not clear yet". Konrad *et al.*[8] found that the size of nanoparticles plays an important role and might explain a variation of about 30 nm in $\lambda_{max}$; however, this does not explain the variation shown in Table 1. Fukabori *et al.*[7] found a relation between the scintillation light output and crystal size in their $Y_2O_3$ samples: the larger the crystallites, the higher the light output.

Table 1 $\lambda_{max}$ of luminescence band of non-doped cubic $Y_2O_3$

| $\lambda_{max}$ (nm) | Type of excitation | Ref. |
|---|---|---|
| 410 | UV: 248 nm | 6 |
| 340 | UV: 207 nm | 8 |
| 344 | UV: 207 nm | 12 |
| 350 | α-particles | 7 |
| 410 | X-ray | 9 |
| 364 | X-ray | 10 |
| 500 | X-ray | 11 |
| 385 | X-ray | 13 |

[a] Centre for Phosphor and Display Materials, Wolfson Centre for Materials Processing, Brunel University London, Uxbridge, Middlesex, UB8 3PH, UK. E-mail: Terry.ireland@brunel.ac.uk
[b] Department of Electronic and Computer Engineering, Brunel University London, Uxbridge, Middlesex, UB8 3PH, UK


This journal is © The Royal Society of Chemistry 2016

Open Access Article. Published on 08 July 2016. Downloaded on 1/16/2026 9:49:37 PM.
This article is licensed under a Creative Commons Attribution 3.0 Unported Licence.

Wood and Hayes[10] reported that the 364 nm emission band is particularly strong upon X-ray excitation at 1.6 K; Tanner *et al.*[12] also found that the 344 nm band in $Y_2O_3$:$Eu^{3+}$ with either 0.1 mol% or 1 mol% $Eu^{3+}$ is strongly temperature dependent.

Besides the position of $\lambda_{max}$ there is another interesting characteristic of the intrinsic luminescence of $Y_2O_3$: the quenching of this luminescence upon doping with rare earth ions. This was first noticed by Wickersheim and Lefever[6] and later by Jacobsohn *et al.*[9] and Tanner *et al.*[12] Jacobson *et al.* observed a strong reduction of the intrinsic $Y_2O_3$ luminescence upon doping with 20 ppm $Tb^{3+}$, while the intrinsic $Y_2O_3$ luminescence virtually disappeared at doping with 0.08 at% $Tb^{3+}$. Hayes *et al.* mention the weak intrinsic luminescence of $Y_2O_3$ upon doping with $Eu^{3+}$.[14] This phenomenon has been observed by other workers as well in studies of $Y_2O_3$ doped with other rare earth ions, although without comment.[15,16] Fukabori *et al.*[15] measured a weak intrinsic band at 350 nm upon doping $Y_2O_3$ with 1 mol% Nd, while Fujimoto *et al.*[16] measured a weak emission band at 360 nm upon doping with 0.15 mol% $Tm^{3+}$. These latter authors assigned this band to the emission of $Tm^{3+}$; however, we believe that the measured emission band is too broad for an emission line of $Tm^{3+}$. Upon exciting $Y_2O_3$:$Eu^{3+}$ (5 mol% $Eu^{3+}$) and $Y_2O_3$:$Tb^{3+}$ (0.5 mol% $Tb^{3+}$) with α-particles, Cress *et al.*[17] could not detect any broad emission band in the near UV-blue. This indicates that at these rare earth concentrations the intrinsic $Y_2O_3$ emission has been quenched completely. Comparing this result with the observation of Hayes *et al.*,[14] it may be concluded that $Tb^{3+}$ is more effectively quenching the intrinsic $Y_2O_3$ luminescence than $Eu^{3+}$. Ato *et al.*[18] reported a strong thermo-luminescence peak of $Y_2O_3$:$Eu^{3+}$ upon irradiation with γ-rays from a $Co^{60}$ source at low and high dose rates. They did not suggest at that time that $Eu^{3+}$ was being reduced by γ-rays: this mechanism was suggested nine years later by Ozawa,[19] a co-author of Ato.[18]

The intrinsic luminescence of $Y_2O_3$ has been explained by three different mechanisms: (1) oxygen vacancies,[9] (2) self-trapped excitons (STE)[7,8,10,12,14,20,21] and (3) ligand-to-metal charge-transfer involving the empty 3d orbitals of the $Y^{3+}$ ion.[13] The latter two mechanisms are more plausible, because luminescence due to STEs[14] or charge-transfer generates broad bands, while Hayes *et al.*[14] also concluded that the STE-mechanism is likely from their measurements of optical detection of magnetic resonance (ODMR). No explanation is apparent in the literature for the quenching of the intrinsic luminescence of $Y_2O_3$ upon doping with rare earth ions.

The current density in a projection CRT at normal operating conditions has a maximum at about 0.25 A $m^{-2}$. There have been no reports of finding blue CL from $Y_2O_3$:$Eu^{3+}$ in such CRTs. In a scanning electron microscope the beam current at the specimen is normally between 0.01 nA and 1 nA, dependent on the settings of the condenser lenses,[22] and the spot size is often of the order of 1.5 nm, leading to current densities between $6 \times 10^6$ A $cm^{-2}$ and $6 \times 10^8$ A $cm^{-2}$, which are 7 to 9 orders of magnitude larger than in a CRT. If the electron transmission at 200 keV is about 99.99% in 200 nm crystals of $Y_2O_3$, then the effective current density is still 3 to 5 orders of magnitude higher. This difference in effective current density could explain why blue emission was never observed before or previously reported. Another reason is the quenching of this emission at $Eu^{3+}$ concentrations greater than 2 mol% (which is typical for CRTs and fluorescent lamps red phosphors). In our laboratories we are currently involved in cathodoluminescence (CL) and photoluminescence (PL) studies of nanosized and submicron $Y_2O_3$ doped with $Eu^{3+}$,$Tb^{3+}$ and other rare earth ions.[23–26] Yttrium oxide is a stable compound and when doped with $Eu^{3+}$, nobody (to our knowledge) has observed broad emission bands between 350 and 500 nm as mentioned above. It was therefore a surprise when investigating $Y_2O_3$:$Eu^{3+}$ samples in our transmission electron microscope (TEM) equipped with an optical spectrometer that we observed a broad emission band at 350 nm. Preliminary results of this observation have been presented at the 22nd International Display Workshops in Japan.[27] Herein we describe further measurements and present an analysis of the intrinsic emission of non-doped $Y_2O_3$ and $Y_2O_3$:$Eu^{3+}$ in the electron beam of a TEM.

## 2. Materials and methods

### Materials and synthesis

Yttrium oxide (99.99%, Ampere Industrie, France) and europium(III) oxide (99.99%, Neo Performance Materials, UK) were used to prepare the europium-doped yttrium nitrate stock solutions. Urea, nitric acid, oxalic acid and isopropanol (IPA) were supplied by (Fisher Scientific, UK). All chemicals were used as received.

The synthesis of sub-micrometre spherical $Y_2O_3$:$Eu^{3+}$ precursor particles *via* a homogeneous precipitation route utilising the hydrothermal decomposition of urea method, followed by annealing the precursor particles at 980 °C resulting in cubic $Y_2O_3$:$Eu^{3+}$ has been described extensively in our earlier work.[23–26] The concentration of $Eu^{3+}$ in $Y_2O_3$ was adjusted to 0.1, 0.5, 1, 1.5, 4, 20, 60 and 100 mol%. For comparison reasons three samples of micrometre sized $Y_2O_3$:$Eu^{3+}$ precursor particles were prepared *via* an oxalate precipitation route.[1,3] The first sample was made by co-precipitation of $Eu^{3+}$-oxalate (2%) and $Y^{3+}$-oxalate. The second and third samples were made by separately precipitating $Y^{3+}$-oxalate and $Eu^{3+}$-oxalate (6% and 2%) and then slurry-mixing (SM) these precipitates before annealing. These samples were then annealed for four hours at 980 °C in air.

### Transmission electron microscope

The submicron spherical $Y_2O_3$ and $Y_2O_3$:$Eu^{3+}$ samples were investigated with a TEM (2100F, JEOL, Japan) equipped with a Schottky-type field emission gun. When operated in scanning mode (STEM), the spot size of the e-beam at the specimen was adjusted to 0.2 nm or 1.5 nm. Initial work demonstrated the need to reduce the X-rays in the column generated from the condenser lens aperture, which were found to significantly contribute to disperse excitation of phosphor samples. These X-rays excited the phosphor and caused the emission of visible

Open Access Article. Published on 08 July 2016. Downloaded on 1/16/2026 9:49:37 PM.
This article is licensed under a Creative Commons Attribution 3.0 Unported Licence.

light when the electron beam was not on the sample, leading to unwanted interference and a loss of resolution. To reduce this X-ray excitation of the sample, a hard X-ray aperture was inserted into the column, which reduced the background noise in CL imaging and spectroscopy modes considerably. The TEM was equipped with a Vulcan™ CL detector, Gatan, USA, for imaging and spectroscopic purposes. This system used a Czerny–Turner spectrometer with back-illuminated CCD and a grating with 1200 lines per mm (blazed at 500 nm) for collection of CL emission spectra. Light was collected from the sample using a mirror above and below the sample, which enabled a solid angle of about 5 sr, which is almost half of a sphere. This high solid angle made light collection highly efficient and enabled the collection of CL at low intensity. Unfortunately, the cooled detector of this spectrometer did not allow the recording of spectra at $\lambda < 380$ nm. In the subsequent sections spectra recorded with this spectrometer will be represented at $\lambda > 400$ nm. Spectra between 200 and 400 nm were recorded with the Black Comet spectrometer of StellarNet Inc. (USA) for undoped $Y_2O_3$. This spectrometer had an uncooled detector and the spectra were therefore much noisier.

By collecting the visible light with the Vulcan system simultaneously with JEOL's high-angle annular dark-field (HAADF) detector, it was possible to observe the visible light that was emitted from the particles. A small cryostat connected to the sample holder enabled cooling of the samples in the TEM down to 102 K (−171 °C); adjustment of the sample temperature anywhere between 102 K and 303 K could be made. A Gatan electron energy loss spectrometer (EELS) was used to map the position of europium ions at the surface of the nanocrystals.

### X-ray powder diffraction

The crystalline phases of the products were determined by X-ray powder diffraction (XRPD) using a Bruker D8 Advance X-ray powder diffractometer fitted with a nickel-filtered copper source and a LynxEye™ silicon strip detector. Data were recorded from 5 to 100 $2\theta$ degrees at 25 °C. The diffractometer was previously calibrated using an aluminium oxide line position standard from Bruker and a $LaB_6$ NIST SRM 660a line profile standard. Diffractograms were collected using the annealed powders in a conventional holder. The emission of the nickel filtered Cu source and hence the instrumental line broadening was determined by fitting the NIST standard using Bruker Topas version 3. Phases in the combusted products were identified from the XRD patterns by peak search matching using the ICCD PDF-2 data files.

## 3. Results

### Transmission electron microscope analysis

Fig. 1a is a TEM image of the urea-precipitated cubic spherical submicron $Y_2O_3$:$Eu^{3+}$ phosphor particles with diameters between 200 nm to 300 nm. Fig. 1b presents a TEM image of a single particle, which is composed of a number of tessellated nanocrystals from 40 nm to 80 nm.

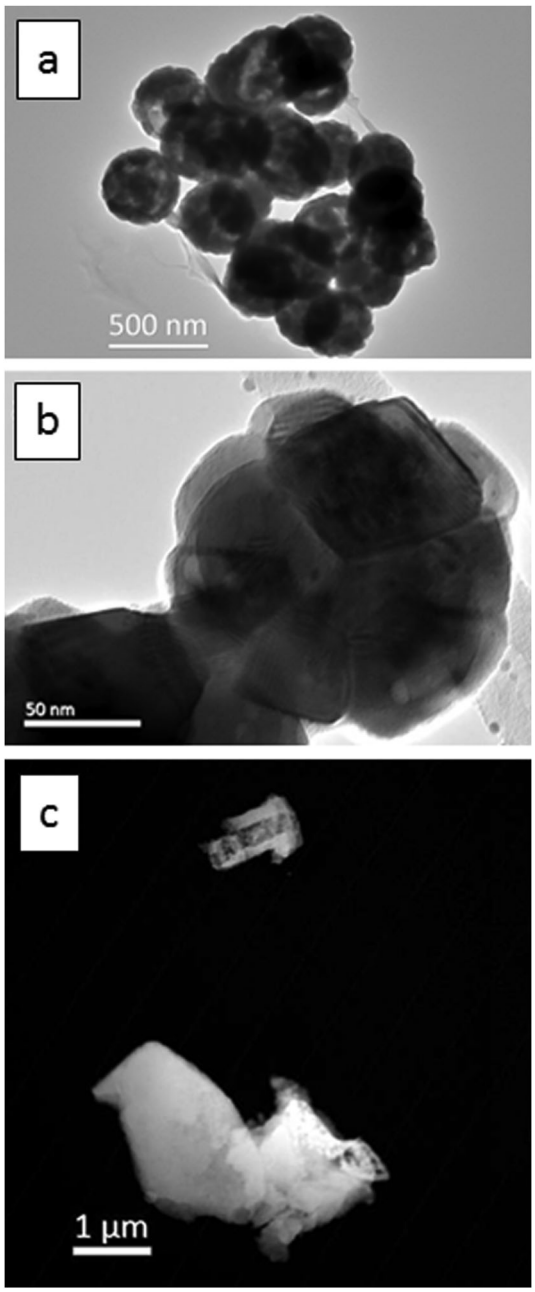


Fig. 1 TEM images, (a) and (b), of $Y_2O_3$:$Eu^{3+}$ particles: (a) urea-precipitated route, (b) higher magnification image of a single particle from (a). (c) HAADF image oxalate-precipitated particles.

In Fig. 1c the oxalate-precipitated cubic micrometre sized $Y_2O_3$:$Eu^{3+}$ phosphor particles are presented. These have an irregular morphology with a size range between 1 and 3 micrometres.

### X-ray diffraction

X-ray diffraction was only used for the analysis of the oxalate-precipitated samples of $Y_2O_3$:$Eu^{3+}$, because urea-precipitated samples of $Y_2O_3$ and $Y_2O_3$:$Eu^{3+}$ after annealing at 980 °C for 4 hours are known to consist of the cubic phase for 100%.[23–26] Fig. 2 shows the diffractogram for oxalate-precipitated $Y_2O_3$:$Eu^{3+}$.

Open Access Article. Published on 08 July 2016. Downloaded on 1/16/2026 9:49:37 PM.
This article is licensed under a Creative Commons Attribution 3.0 Unported Licence.

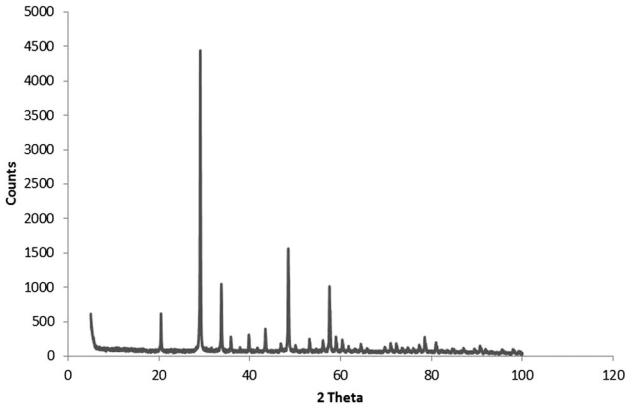


Fig. 2 Powder X-ray diffractogram of $Y_2O_3$:$Eu^{3+}$ (2%) oxalate method co-precipitated. Fired at 980 °C for 4 hours.

This diagram proved that this material after annealing for 4 hours at 980 °C also consisted for >99% of the cubic phase.

### UV/blue emission band

Fig. 3 shows a spectrum of undoped $Y_2O_3$ excited with an electron beam of 200 keV at −120 °C. The as-recorded spectrum is the noisy curve (1), which is represented by a Gaussian profile (3) corrected for the background (2). The Gaussian profile has been fitted to the spectrum with a least squares algorithm using Microsoft's Excel solver.

By averaging the values for $\lambda_{max}$ and the full width at half maximum (FWHM) from spectra recorded at various temperatures, we determined that $\lambda_{max}$ = 353 nm (28 300 $cm^{-1}$) and FWHM = 5735 $cm^{-1}$. This value of $\lambda_{max}$ is identical to the value published by Fukabori *et al.*[7] and close to the values published by Konrad *et al.*,[8] Wood and Hayes[10] and Tanner *et al.*[12] Fukabori *et al.* found that in some of their samples the emission extended much further in the visible region. This has not been confirmed in our measurements, neither in those of the other workers.[8–10,12,13] Nevertheless, the broad UV emission band represented in Fig. 4 extends substantially into the visible part of electromagnetic radiation. At 405 nm the

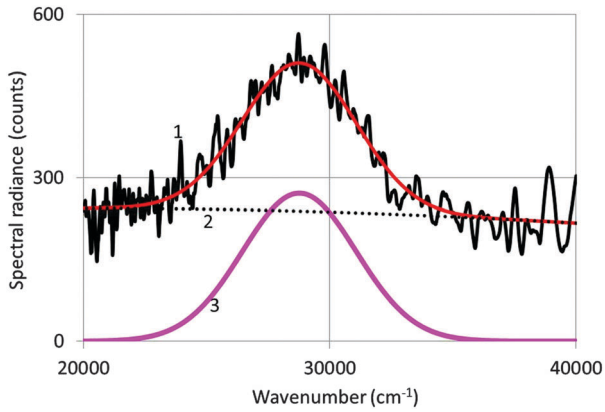


Fig. 3 Spectrum of undoped $Y_2O_3$ excited with an electron beam of 200 keV and spot size 1.5 nm at −120 °C (1). Recorded with the StellarNet spectrometer with an integration of 16 s. (2): Background. (3): Gaussian profile fitted to the data points and corrected for background.

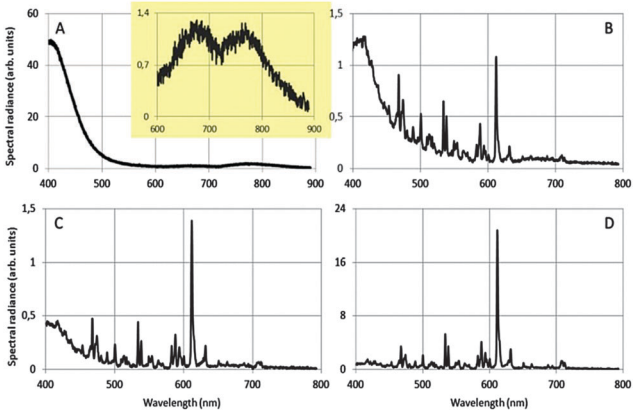


Fig. 4 CL spectra of $Y_2O_3$:$Eu^{3+}$ recorded at −171 °C, 200 keV beam voltage and spot size of 1.5 nm. (A) non-doped $Y_2O_3$, inset: spectrum at larger scale between 600 nm and 900 nm; (B) 0.1 mol% $Eu^{3+}$; (C) 0.5 mol% $Eu^{3+}$; (D) 1 mol% $Eu^{3+}$. The sharp lines in the spectrum are $Y_2O_3$:$Eu^{3+}$ transitions; the strongest is the $^5D_0 \rightarrow {}^7F_2$ $Eu^{3+}$ transition at 611 nm.

spectral radiance is almost 5 times smaller than at 353 nm; however, for comparing the intrinsic $Y_2O_3$ luminescence with the $Eu^{3+}$ emission lines for the doped samples, we used the Gatan spectrometer with the cutoff at about 390 nm, basically because of the detector limitation of the StellarNet spectrometer.

Fig. 4 shows how we were able to turn the red-emitting phosphor $Y_2O_3$:$Eu^{3+}$ into a UV/blue-emitting phosphor in the TEM: the radiance of the UV/blue luminescence is dwarfing the (area) radiance of the well-known emission lines of $Eu^{3+}$ in $Y_2O_3$ at 0.1 mol% $Eu^{3+}$. Important conditions for observing the broad UV luminescence are: low temperature of the sample: −171 °C, large spot size of the e-beam of 1.5 nm, high beam current by maximising the condenser lens aperture and a specimen thickness of at least 100 nm. The energy of the electron beam does not seem paramount: we observed the UV/blue luminescence both at 200 keV at 80 keV. In Fig. 4A the sharp emission lines of $Eu^{3+}$ are not present: whereas the strongest transition in Fig. 4B–D is that due to the $^5D_0 \rightarrow {}^7F_2$ $Eu^{3+}$ transition at 611 nm. The vertical scales of the graphs in Fig. 4 cannot be compared due to the different integration times during spectra recording and different specimen thicknesses. It can be seen that the spectral radiance (normalised to the spectral radiance at 611 nm) of the blue emission at 400 nm decreases strongly when the concentration of $Eu^{3+}$ is increased from 0.1 to 1 mol%. At $Eu^{3+}$ concentrations ≥2 mol% in urea-precipitated $Y_2O_3$:$Eu^{3+}$ we could not detect any UV/blue emission at 400 nm. Beside the strong UV/blue emission at 400 nm, two very weak long wavelength bands can be observed (inset of Fig. 4A), one at about 675 nm and the other at about 770 nm. Electron bombardment of the carbon-coated Cu-grid without $Y_2O_3$:$Eu^{3+}$ particles did not show any CL; hence, interference from the Cu-grid holder material can be excluded.

The luminescence spectrum between 400 nm and 500 nm in Fig. 4A (and the weak long wavelength bands) did not noticeably change its shape upon reducing the energy of the electron beam from 200 keV to 80 keV. This therefore excludes Cherenkov radiation being the origin of the observed emission bands at

Open Access Article. Published on 08 July 2016. Downloaded on 1/16/2026 9:49:37 PM.
This article is licensed under a Creative Commons Attribution 3.0 Unported Licence.

353 nm, 675 nm and 770 nm.[28] At 400 nm the refractive index of $Y_2O_3$ is 1.98: to calculate the refractive index of $Y_2O_3$ as a function of $\lambda$, use was made of the dispersion formula given by Nigara.[29] The condition for Cherenkov radiation in a medium with a refractive index of 1.98 is satisfied when the electron velocity $>1.52 \times 10^8$ m s$^{-1}$, which starts at an electron energy of 80 keV. So, at 80 keV there cannot be Cherenkov radiation in $Y_2O_3$ at wavelengths $>\sim 405$ nm. From this straightforward calculation it can be concluded that any light at wavelengths $>405$ nm that is emitted upon bombarding non-doped, transparent $Y_2O_3$ crystals with electrons at 80 keV cannot be ascribed to Cherenkov radiation. Since the position and shape of the blue emission did not change upon increasing the electron energy to 200 keV, we can reasonably exclude Cherenkov radiation for 200 keV electrons as well. Additional evidence for this conclusion is the strong temperature dependence of the UV/blue and red emission, as we shall discuss in the following paragraphs. Cherenkov radiation is virtually not affected by temperature as long as the refractive index and the density of the specimen do not change substantially. In ref. 27 it was supposed that the blue emission of $Y_2O_3$:$Eu^{3+}$ at 400 nm was caused by reduction of $Eu^{3+}$ to $Eu^{2+}$. From Fig. 4A it must be concluded that this is not the case and that the blue emission in all graphs of Fig. 4 is intrinsic luminescence of $Y_2O_3$. In other words, it is concluded that the UV/blue luminescence observed in the TEM is identical to the blue/UV emission from undoped $Y_2O_3$ and $Y_2O_3$ doped with small amounts of rare earth ions upon excitation by other sources of ionizing radiation.[7–16]

In order to quantify the quenching of the intrinsic luminescence of $Y_2O_3$ upon increasing the $Eu^{3+}$ concentration we define a quenching factor $\eta$:

$$\eta = \frac{SR_{405}}{SR_{405} + SR_{611}}, \quad (1)$$

where $SR_{405}$ is the spectral radiation of the UV/blue emission at 405 nm and $SR_{611}$ is the spectral radiance of the $^5D_0 \rightarrow {}^7F_2$ $Eu^{3+}$ transition at 611 nm. For non-doped $Y_2O_3$ $\eta = 1$ and for $Eu^{3+}$ concentrations $>2$ mol%, $\eta = 0$.

Fig. 4B–D refer to $Y_2O_3$ doped with 0.1, 0.5 and 1 mol% $Eu^{3+}$. Apart from the diminishing intrinsic luminescence of the host material there is another interesting phenomenon, *viz.* the changing ratios between the spectral radiance of the strongest $Eu^{3+}$ transition at 611 nm and the spectral radiances of $Eu^{3+}$ transitions at $\lambda < 611$ nm. Furthermore, these latter transitions are about two orders of magnitude stronger than the corresponding transitions in the photoluminescence (PL) spectrum of $Y_2O_3$:$Eu^{3+}$ as represented in Ozawa's book on page 165.[3] We shall discuss these phenomena together with the intrinsic luminescence of $Y_2O_3$ in the next section.

Fig. 5 is a HAADF image of urea-precipitated $Y_2O_3$:$Eu^{3+}$ (0.1 mol% $Eu^{3+}$) at −168 °C and 200 keV. The image illustrates the effect of positioning of the e-beam on $\eta$. The square denoted by "Spatial Drift" indicates the image that was used to compensate the thermal drift of the sample holder during cooling and warming up. This feature enabled a stable position of the electron beam on the nanocrystal during recording of the spectra, which required more than 2 minutes in some cases. The sites SI.1 to SI.5 in Fig. 5 refer to spots with different particle thickness: SI.1 is a very small particle, whereas SI.2 and SI.3 refer to spots with two particles on top of each other.

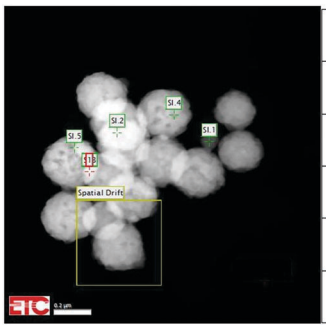


| Site | $SR_{405}$ | $SR_{612}$ | η |
|---|---|---|---|
| SI-1 | 0.5 | 2.6 | 0.16 |
| SI-2 | 12.2 | 10.8 | 0.53 |
| SI-3 | 5.3 | 10.2 | 0.34 |
| SI-4 | 3.3 | 5.6 | 0.37 |
| SI-5 | 2.5 | 8.4 | 0.23 |

Fig. 5 Quenching factor $\eta$ at various sites for urea-precipitated $Y_2O_3$:$Eu^{3+}$ (0.1 mol% $Eu^{3+}$) at −168 °C and 200 keV.

This is reflected in the rather high value for the $Eu^{3+}$ emission. In the other urea-precipitated samples of $Y_2O_3$:$Eu^{3+}$ containing larger $Eu^{3+}$ concentrations, the variation of the quenching factor $\eta$ was less than a factor of two. Since some $Y_2O_3$:$Eu^{3+}$ particles are partially hollow, it is impossible to determine a relation between $R_{405}$ and $R_{611}$ and specimen thickness from Fig. 5. It should be kept in mind that the radiance $R_b$ of the $Y_2O_3$ emission band, defined as

$$R_b = \int_{b-}^{b+} SR(\lambda)d\lambda \quad (2)$$

where $b-$ and $b+$ are the integration limits, is outstripping the radiance of the $^5D_0 \rightarrow {}^7F_2$ $Eu^{3+}$ transition at 611 nm at low $Eu^{3+}$ concentrations, because the UV emission band is much broader than the 611 nm peak.

Fig. 6 shows the effect of temperature on the spectral radiance of the intrinsic emission of undoped $Y_2O_3$: the lower the temperature, the stronger the UV/blue luminescence. The drift corrector facility, indicated in Fig. 5, guaranteed that the spectra shown in Fig. 6 were recorded at the same spot. Since the time for recording the spectra (integration time) was also kept constant, the spectra for different temperatures can be compared directly: *i.e.* there is no effect of thickness. The intrinsic blue luminescence in $Y_2O_3$:$Eu^{3+}$ also increased by more than a factor of 10 upon decreasing the temperature from 31 °C to −171 °C.

The two long wavelength bands shown in the inset of Fig. 6 are much weaker than the UV/blue emission and are also stronger at −172 °C than at 30 °C. It can be seen that the temperature behaviour of the band at 675 nm deviates from that of the other band at 770 nm and the UV/blue band. Upon excitation of $Y_2O_3$ or $Y_2O_3$:$Eu^{3+}$ by X-rays or α-particles no emission was observed from these bands by other workers.[7,9–11,13–16] These bands also disappeared when the $Eu^{3+}$ concentration was increased. The origin of these two bands is unknown.

Fig. 7 is an Arrhenius plot of the spectral radiance (SR) measured at 353 nm with the StellarNet spectrometer (data points 1) and SRs measured at 405 nm with the Gatan

Open Access Article. Published on 08 July 2016. Downloaded on 1/16/2026 9:49:37 PM.
This article is licensed under a Creative Commons Attribution 3.0 Unported Licence.

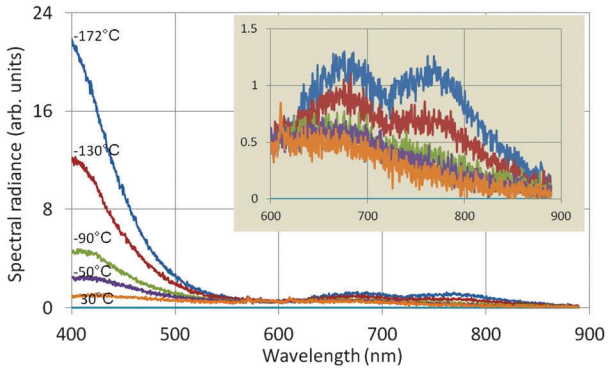


Fig. 6 Spectra of undoped $Y_2O_3$ recorded at 80 keV and various temperatures. The inset shows the spectra between 600 and 900 nm at a different vertical scale.

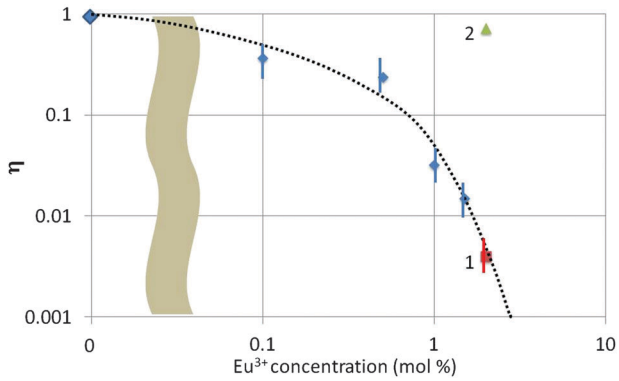


Fig. 8 Quenching factor $\eta$ as a function of $Eu^{3+}$ concentration in $Y_2O_3$. (1): oxalate-co-precipitated $Y_2O_3$:$Eu^{3+}$, (2) SM-oxalate-precipitated $Y_2O_3$:$Eu^{3+}$. Other points refer to urea-precipitated samples. The abscissa is quasi-logarithmic, because the point with 0 mol% $Eu^{3+}$ dope has been indicated.

spectrometer (data points 2 and 3). The data points of (1) refer to undoped $Y_2O_3$ and 200 keV beam energy, the data points of (2) refer also to undoped $Y_2O_3$ but at 80 keV and the data points of (3) refer to $Y_2O_3$:$Eu^{3+}$ with 0.1 mol% $Eu^{3+}$ and 200 keV. The drift corrector facility enabled us to stay at the same point during recording of the spectra and after changing the temperature. In some cases a tiny shift was applied to deal with beam degradation. However, the measured effect of beam degradation on spectral radiance was $<2\%$, which was smaller than the noise level in the spectra, especially in the StellarNet spectra, as shown in Fig. 3. The curves in Fig. 7 have been fitted to the data points with eqn (4) that describes the temperature-dependent effect of STEs. This will be discussed in the next section. The trap depth that describes the experimental data for non-doped $Y_2O_3$ is 0.13 eV and it is 0.16 eV for $Y_2O_3$:$Eu^{3+}$ with 0.1 mol% $Eu^{3+}$. For $Y_2O_3$:$Eu^{3+}$ with other $Eu^{3+}$ concentrations the Arrhenius plots are similar to that of 0.1 mol% $Eu^{3+}$ as indicated in Fig. 7. In view of the spread in the data we consider that the trap depth of the STEs in undoped and doped $Y_2O_3$ is identical and has a value of 0.14 eV.

In Fig. 8 we have summarized the quenching factor $\eta$ (for the blue band) as a function of $Eu^{3+}$ concentration for all samples

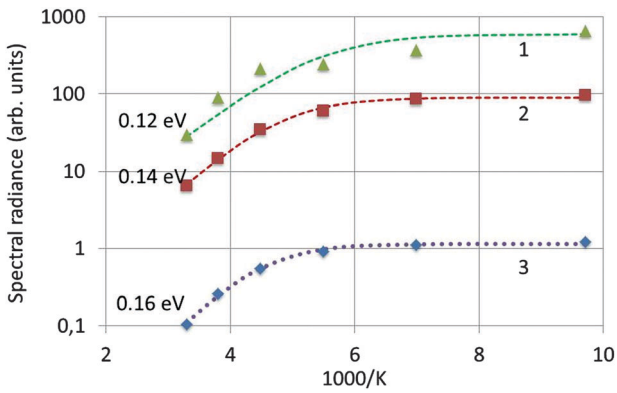


Fig. 7 Arrhenius plot of spectral radiance *versus* 1000 K. (1): $SR_{353}$ of undoped $Y_2O_3$ recorded at 200 keV; (2): $SR_{405}$ of undoped $Y_2O_3$ recorded at 80 keV; (3): $SR_{405}$ of $Y_2O_3$:$Eu^{3+}$ with 0.1 mol% $Eu^{3+}$ recorded at 200 keV. The dashed curves have been fitted to the experimental data with eqn (4).

investigated in the TEM. There are three types of samples collected in Fig. 8, *viz.* urea-precipitated (without a number), oxalate co-precipitated (no. 1) and SM-oxalate precipitated (no. 2). As mentioned above, blue luminescence could not be observed for the urea-precipitated samples at $Eu^{3+}$ concentrations $>1.5$ mol%, whereas the SM-oxalate samples showed very large blue luminescence for 2 and 6 mol% $Eu^{3+}$. The spread in $\eta$ was about a factor of 3 in the SM-oxalate samples; in the urea-precipitated samples it was less.

Fig. 8 illustrates the different behaviour of the SM-oxalate-precipitated and urea-precipitated samples, whereas the oxalate co-precipitated sample (point 1 in Fig. 8) with molecular mixing of the $Eu^{3+}$ and $Y^{3+}$ ions indicates that this sample behaves as the urea-precipitated samples. The deviating behaviour of the SM-oxalate-precipitated sample is explained by its inhomogeneity, in which $Eu^{3+}$-rich areas in the crystals are alternating with areas with very low $Eu^{3+}$ concentration. The penetration depth of 200 keV electrons in crystalline $Y_2O_3$ is about 75 μm,[5,30] which is much larger than the size of the oxalate-precipitated crystals. The $Eu^{3+}$ rich areas in the crystal hit by the e-beam do not contribute to the build-up of the blue band because of concentration quenching, whereas the areas with very low $Eu^{3+}$ concentration take care of the strong blue band signal. This hypothesis was confirmed by the very low $Eu^{3+}$ signal in the EELS (not shown) at various spots. From this consideration it can be concluded that the SM-oxalate precipitated sample should be inserted at a much lower concentration in Fig. 8. Since the effective $Eu^{3+}$ concentration is unknown, the best we could do is plotting the result at the as-made $Eu^{3+}$ concentration.

Finally we would like to mention that we also observed blue luminescence in the TEM when bombarding undoped monoclinic $Y_2O_3$ crystals with 200 keV electrons at 1.5 nm spot size. The monoclinic material was unstable under these electron bombardment conditions, decomposing partly into the more stable cubic form, and therefore we do not reproduce any results of these measurements in this article.

Open Access Article. Published on 08 July 2016. Downloaded on 1/16/2026 9:49:37 PM.
This article is licensed under a Creative Commons Attribution 3.0 Unported Licence.

### Discussion of blue luminescence in $Y_2O_3$ and transition ratios

When an electron beam of 200 keV hits an $Y_2O_3$ crystal it produces besides defects, backscattered and secondary electrons, X-rays and holes by inelastic scattering processes. Electrons and holes can combine to form free excitons and STEs. Herein we adopt the model that STEs are responsible for the blue luminescence in undoped $Y_2O_3$ and $Y_2O_3$:$Eu^{3+}$ as indicated in the literature.[7,8,10,12,14,20,21] According to Mikhailik and Kraus[31] and Blasse[32] the radiance $B$ of a scintillator upon excitation can be written as:

$$B = \alpha N_{e\text{–}h} S Q \quad (3)$$

where $\alpha$ is a proportionality constant, $N_{e\text{–}h}$ is the number of electron–hole pairs that is generated by the electron beam inside the crystal, $S$ is the probability of transferring energy from an e–h pair to a luminescent centre, *e.g.* a $Eu^{3+}$ ion, and $Q$ is the luminescence quantum efficiency. Undoped $Y_2O_3$ is a so-called self-activated or intrinsic scintillator,[31] in which $S$ is 1 by definition. The intrinsic luminescence in non-doped $Y_2O_3$ is considered to come from O-2p levels and Y-3d levels after an STE has combined with a luminescent centre in $Y_2O_3$.[11] The quantum efficiency $Q$ in eqn (3) can be described by Mott's equation on thermal quenching:[31]

$$Q = \frac{P}{1 + Ce^{-E_A/kT}} \quad (4)$$

where $P$ and $C$ are constants to be fitted, $E_A$ is the activation or trap energy, $k$ is Boltzmann's constant and $T$ is the absolute temperature. In Fig. 8 we have fitted $Q$ according to eqn (4) to the experimental points for undoped $Y_2O_3$ and $Y_2O_3$:$Eu^{3+}$ with 0.1 mol% $Eu^{3+}$. It can be seen that the experiments are satisfactorily represented with $E_A$ = 0.14 eV both for non-doped $Y_2O_3$ and 0.1 mol% $Y_2O_3$:$Eu^{3+}$. We interpret this activation energy as the trap depth of the self-trapped exciton.

It should be kept in mind that eqn (3) for self-activated $Y_2O_3$ refers to the radiance of the blue emission band. When $Y_2O_3$ is doped with $Eu^{3+}$, energy will be transferred from the host lattice to the $Eu^{3+}$ luminescent centres: hence, the CL spectrum of $Y_2O_3$:$Eu^{3+}$ can be detected. The CL of $Y_2O_3$:$Eu^{3+}$ can also be described with an energy transfer probability $S$ in eqn (3), which is 0 for undoped $Y_2O_3$ and has a maximum value, albeit $< 1$, for a dopant concentration of 2 mol% and larger.

As mentioned above, Fig. 4 shows that the spectral radiance of $Eu^{3+}$ transitions at $\lambda < 580$ nm decreases in the sequence Fig. 4B–D. We have plotted this behaviour for some transitions in Fig. 9.

Fig. 9 represents the ratios $R_1$ and $R_2$, which are the ratios of the spectral radiances $^5D_1 \rightarrow {}^7F_1$ (533 nm) and $^5D_0 \rightarrow {}^7F_2$ (611 nm) and that of $^5D_0 \rightarrow {}^7F_4$ (713 nm) and $^5D_0 \rightarrow {}^7F_2$ (611 nm) respectively. It can be seen that $R_1$ decreases almost by a factor of 10 upon increasing the dopant concentration from 0.1 mol% to 4%, whereas $R_2$ is constant, both at cryogenic and room temperature. The latter ratio is constant, because it refers to $^5D_0$ transitions. The transitions of the $^5D_2$ and $^5D_3$ states to the $^7F_J$ manifold show a similar behaviour as the $^5D_1 \rightarrow {}^7F_1$ transition; however, due to the lower spectral radiances the error bar in the graphs is larger and therefore these will not be reproduced here. The partial concentration quenching of the $^5D_1$ transition of the $Eu^{3+}$ ion represented in Fig. 9 is well known and it has been described by Blasse and Grabmaier[2] and Klaassen *et al.*[33] Blasse and Grabmaier explained the behaviour of $R_1$ in terms of the following cross relaxation in $Eu^{3+}$:

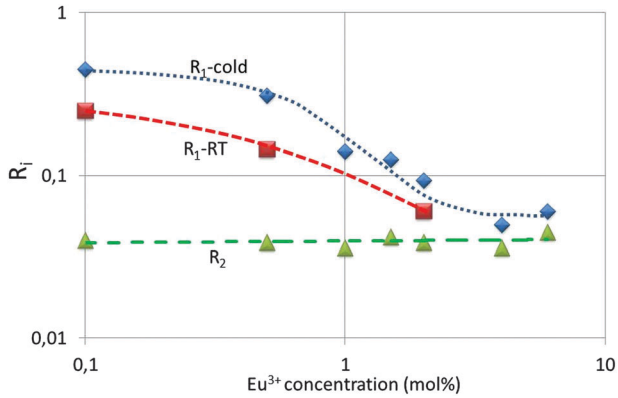


Fig. 9 Ratio of spectral radiance between $^5D_1 \rightarrow {}^7F_1$ (533 nm) and $^5D_0 \rightarrow {}^7F_2$ (611 nm): $R_1$ and ratio of spectral radiance between $^5D_0 \rightarrow {}^7F_4$ (713 nm) and $^5D_0 \rightarrow {}^7F_2$ (611 nm): $R_2$. For $R_1$ the measurements at −170 °C (cold) and room temperature (RT) gave different results.

$$^5D_1 + {}^7F_0 \rightarrow {}^5D_0 + {}^7F_3. \quad (5)$$

This cross relaxation is facilitated by the ten times faster decay rate from $^5D_1$ levels as that from $^5D_0$ levels as indicated by Klaassen *et al.*[33] These latter authors described the partial quenching of $^5D_J$ (for $J > 0$) transitions in terms of radiative decay time and the rate of non-radiative transfer processes. However, neither cross relaxation nor rate constants explain why $R_1$ is so large in Fig. 9 at low $Eu^{3+}$ concentrations.

For a qualitative explanation we shall make use of the energy diagram depicted in Fig. 10. Most levels indicated in Fig. 10 have been reported by Wen *et al.*,[34] only the lowest energy level of the manifolds is indicated. The energy level of the intrinsic $Y_2O_3$ emission band has been centred at 28 300 $cm^{-1}$ above the ground level $^7F_0$ of $Eu^{3+}$, based on the spectrum depicted in Fig. 4. The level of the STE $Y_2O_3$ emission band overlaps with several $Eu^{3+}$ levels; hence, it seems obvious that energy can radiationless be transferred from an STE in $Y_2O_3$ to the $^5D_4$ level of $Eu^{3+}$, which is only slightly lower. This process, which takes place at $Eu^{3+}$ concentrations >2 mol%, is indicated by arrow 4. From the $^5D_4$ level energy will radiationless trickle down to the $^5D_3$, $^5D_2$, $^5D_1$ and $^5D_0$ levels, indicated by arrows 7. As mentioned above, the decay times of transitions from $^5D_J$ levels with $J > 0$ are about 10 times shorter than these from $^5D_0$,[33] which enhances efficient energy transfer and hence rather fast quenching of the $Y_2O_3$ emission upon increasing the $Eu^{3+}$ concentration.[2,35] In terms of the probability $S$ in eqn (3) it means that energy from an e–h pair is transferred to a $Eu^{3+}$ ion.

At low $Eu^{3+}$ concentrations <2 mol% the strong intrinsic emission at 28 300 $cm^{-1}$ may be absorbed by $Eu^{3+}$ ions in the lattice: this process is indicated by arrows (5) and (6) in Fig. 10. It has been indicated in this figure that the $Y_2O_3$ UV radiation is

Open Access Article. Published on 08 July 2016. Downloaded on 1/16/2026 9:49:37 PM.
This article is licensed under a Creative Commons Attribution 3.0 Unported Licence.

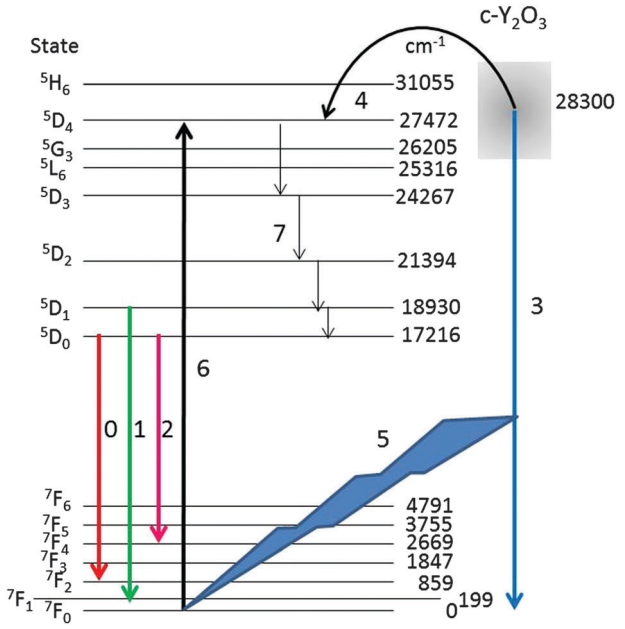


Fig. 10 Energy levels of $Eu^{3+}$ in $Y_2O_3$. The broad intrinsic luminescence of $Y_2O_3$ has been represented at 28 300 $cm^{-1}$ by arrow (3). The arrows (0), (1) and (2) refer to the $^5D_0 \rightarrow {}^7F_2$, $^5D_1 \rightarrow {}^7F_1$ and $^5D_0 \rightarrow {}^7F_4$ $Eu^{3+}$ transitions respectively, while (4) indicates the radiationless energy transfer from $Y_2O_3$ to $Eu^{3+}$. For arrows (5), (6) and (7) we refer to text.

absorbed from the ground level $^7F_0$; hence, the $^5D_4$ $Eu^{3+}$ level will be populated more densely. As mentioned above, from $^5D_4$ energy will trickle down to the lower $^5D_J$ levels. The process indicated by arrows (5) and (6) will stop when the intrinsic luminescence of $Y_2O_3$ has quenched at large $Eu^{3+}$ concentration. The latter process explains the high value of $R_1$ in Fig. 9 and similarly the rather strong $^5D_1 \rightarrow {}^7F_J$ and $^5D_2 \rightarrow {}^7F_J$ transitions in Fig. 4B–D. The foregoing consideration also explains why the ratio $R_1$ in Fig. 9 at low temperature is higher than at room temperature: the process indicated by the arrows (5) and (6) is more dominant at low temperature because of the much stronger UV luminescence of $Y_2O_3$.

## 4. Conclusions

In the preceding sections we have described the cathodoluminescence of undoped $Y_2O_3$ and $Y_2O_3$:$Eu^{3+}$ crystals in the TEM by high-energy electron bombardment. At low temperatures we observed a broad emission band at about 353 nm, which has been ascribed to the migration of excitons to luminescence centres in $Y_2O_3$. We found that the UV/blue luminescence is strongly temperature dependent and that at concentrations $>2$ mol% $Eu^{3+}$ no blue light could be detected.

The temperature behaviour of the intrinsic luminescence of $Y_2O_3$ has been explained with a model for the self-trapped excitons. The depth of these traps was found to be 0.14 eV. The concentration dependence of the UV/blue luminescence has been explained by the good overlap between the level of the blue $Y_2O_3$ band and the $^5D_4$ level of the $Eu^{3+}$ ion. The strong radiance of $^5D_1 \rightarrow {}^7F_J$ and $^5D_2 \rightarrow {}^7F_J$ $Eu^{3+}$ transitions in the spectra excited at 200 keV in $Y_2O_3$:$Eu^{3+}$ with low $Eu^{3+}$ concentration has been explained by absorption of the intrinsic $Y_2O_3$ radiation by $Eu^{3+}$ ions. Although we have presented a detailed explanation of the concentration and temperature behaviour of the UV/blue emission, we have also generated new questions. The most important is about the nature of the red emission bands at 675 nm and 770 nm.

Based on the results described in this article we would like to make a suggestion to other scientists working with electron microscopes in the field of biomedical imaging with phosphors. This fast growing technology has recently been reviewed by Gai *et al.*[36] Since undoped $Y_2O_3$ or $Y_2O_3$:$Eu^{3+}$ with low $Eu^{3+}$ concentration will manifest the strong intrinsic luminescence of $Y_2O_3$ in the e-beam of a TEM (and likely also in a SEM) at low temperatures, we think that this work opens new perspectives for labelling (biological) samples with nanocrystals of $Y_2O_3$:$Eu^{3+}$.

## Acknowledgements

We are grateful to the EPSRC and the Technology Strategy Board (TSB) for funding the PURPOSE (TP11/MFE/6/I/AA129F; EPSRC TS/G000271/1), CONVERTED (JeS no. TS/1003053/1) and PRISM (EP/N508974/1) programs. We are also grateful to the TSB for funding the CONVERT program.

## References

1 *Phosphor Handbook*, ed. W. Yen, S. Shionoya and H. Yamamoto, CRC Press, Boca Raton, 2nd edn, 2007.
2 G. Blasse and B. C. Grabmaier, *Luminescent Materials*, Springer-Verlag, Berlin, 1994.
3 L. Ozawa, *Cathodoluminescence, Theory and Applications*, Kodansha & VCH, Verlag, Tokyo, 1990.
4 G. Li and J. Lin, *Chem. Soc. Rev.*, 2014, **43**, 7099.
5 D. den Engelsen, P. G. Harris, T. G. Ireland and J. Silver, *ECS J. Solid State Sci. Technol.*, 2014, **3**, R53.
6 K. A. Wickersheim and R. A. Lefever, *J. Electrochem. Soc.*, 1964, **111**, 47.
7 A. Fukabori, L. An, A. Ito, V. Chani, K. Kamada, A. Yoshikawa, T. Ikegami and T. Goto, *Ceram. Int.*, 2012, **38**, 2119.
8 A. Konrad, U. Herr, R. Tidecks, F. Kummer and K. Samwer, *J. Appl. Phys.*, 2001, **90**, 3516.
9 L. G. Jacobsohn, B. L. Bennett, R. E. Muenchausen, J. F. Smith and D. W. Cooke, *Proc. SPIE*, 2006, **6321**, 63210J.
10 R. L. Wood and W. Hayes, *J. Phys. C: Solid State Phys.*, 1982, **15**, 7209.
11 T. C. de Oliveira, M. Souza da Silva, L. Menezes de Jesus, D. Vieira Sampaio, J. C. Alves dos Santos, N. R. da Silva Souza and R. Santos da Silva, *Ceram. Int.*, 2014, **40**, 16209.
12 P. A. Tanner, L. Fu and B. M. Cheng, *J. Phys. Chem. C*, 2009, **113**, 10773.
13 G. Blasse and L. H. Brixner, *Eur. J. Solid State Inorg. Chem.*, 1991, **28**, 767.

Open Access Article. Published on 08 July 2016. Downloaded on 1/16/2026 9:49:37 PM.
This article is licensed under a Creative Commons Attribution 3.0 Unported Licence.

14 W. Hayes, M. J. Kane, O. Salminen and A. I. Kuznetsov, *J. Phys. C: Solid State Phys.*, 1984, **17**, L383.
15 A. Fukabori, V. Chani, J. Pejchal, K. Kamada, A. Yoshikawa and T. Ikega, *Opt. Mater.*, 2011, **34**, 452.
16 Y. Fujimoto, T. Yanagida, Y. Yokota, A. Ikesue and A. Yoshikawa, *Opt. Mater.*, 2011, **34**, 448.
17 C. D. Cress, C. S. Redino, B. J. Landi and R. P. Raffaelle, *J. Solid State Chem.*, 2008, **181**, 2041.
18 Y. Ato, R. Huzimura and L. Ozawa, *Jpn. J. Appl. Phys.*, 1968, **7**, 1497.
19 L. Ozawa, *Appl. Phys. Lett.*, 1977, **31**, 694.
20 W. Hayes, *J. Lumin.*, 1984, **31**, 99.
21 A. Lushchik, M. Kirm, Ch. Lushchik, I. Martinson and G. Zimmerer, *J. Lumin.*, 2000, **87–89**, 232.
22 D. B. Williams and C. B. Carter, *Transmission Electron Microscopy, A Textbook for Materials Science*, Springer, New York, 2009.
23 D. den Engelsen, P. G. Harris, T. G. Ireland and J. Silver, *ECS J. Solid State Sci. Technol.*, 2015, **4**, R1.
24 D. den Engelsen, P. G. Harris, T. G. Ireland, R. Withnall and J. Silver, *ECS J. Solid State Sci. Technol.*, 2013, **2**, R201.
25 X. Jing, T. Ireland, C. Gibbons, D. J. Barber, J. Silver, A. Vecht, G. Fern, P. Trogwa and D. C. Morton, *J. Electrochem. Soc.*, 1999, **146**, 4654.
26 J. Silver, T. G. Ireland and R. Withnall, *J. Electrochem. Soc.*, 2004, **151**, H66.
27 G. R. Fern, A. Lipman, J. Silver, A. Howkins, T. G. Ireland, P. Marsh, D. den Engelsen, *Proceedings of 22nd International Display Workshops*, December 9–11, Otsu, Japan, 2015.
28 J. V. Jelley, *Čerenkov Radiation and its applications*, Pergamon Press, London, 1958.
29 Y. Nigara, *Jpn. J. Appl. Phys.*, 1968, **7**, 404.
30 D. den Engelsen, P. G. Harris, T. G. Ireland and J. Silver, *ECS J. Solid State Sci. Technol.*, 2015, **4**, R1.
31 V. B. Mikhailik and H. Kraus, *Phys. Status Solidi B*, 2010, **247**, 1583.
32 G. Blasse, *J. Lumin.*, 1994, **60–61**, 930.
33 D. B. M. Klaasen, R. A. M. van Ham and T. G. M. van Rijn, *J. Lumin.*, 1989, **43**, 261.
34 J. Wen, L. Hu, M. Yin and S. Xia, *Current Appl. Phys.*, 2012, **12**, 732.
35 D. L. Dexter, *J. Chem. Phys.*, 1953, **21**, 836.
36 S. Gai, C. Li, P. Yang and J. Lin, *Chem. Rev.*, 2014, **114**, 2342.

 This journal is © The Royal Society of Chemistry 2016